Journal of Environmental Management 371 (2024) 123235

Contents lists available at ScienceDirect

Journal of Environmental Management

journal homepage: www.elsevier.com/locate/jenvman

Research article

Resveratrol alleviates Mono-2-ethylhexyl phthalate-induced mitophagy, ferroptosis, and immunological dysfunction in grass carp hepatocytes by regulating the Nrf2 pathway☆

Xiaodan Wang [a], Meichen Gao [a], Xiunan Lu [a], Yutian Lei [a], Jiatong Sun [a], Mengyao Ren [a], Tong Xu [a,**], Hongjin Lin [a,b,c,*]

[a] College of Veterinary Medicine, Northeast Agricultural University, Harbin, 150030, China
[b] Key Laboratory of the Provincial Education Department of Heilongjiang for Common Animal Disease Prevention and Treatment, College of Veterinary Medicine, Northeast Agricultural University, Harbin, 150030, China
[c] Laboratory of Embryo Biotechnology, College of Life Science, Northeast Agricultural University, Harbin, 150030, China

ARTICLE INFO

Keywords:
MEHP
Resveratrol
L8824 cells
Nrf2
Mitophagy
Ferroptosis
Immune dysfunction

ABSTRACT

Mono-2-ethylhexyl phthalate (MEHP) is the major biologically active metabolite of Di(2-ethylhexyl) phthalate (DEHP). This MEHP mono-ester metabolite can be transported through the bloodstream into tissues such as the liver, kidneys, fat, and testes and cause corresponding damage. Resveratrol (RSV) has anti-inflammatory, antioxidant, and detoxification characteristics. Our research examined whether RSV alleviates MEHP-induced grass carp hepatocyte (L8824 cell) injury and its relationship with the Nrf2 pathway, mitophagy, ferroptosis, and immune function. Therefore, we treated L8824 cells with 85 μM MEHP and/or 2 μM RSV. The findings indicated that exposing MEHP resulted in increased reactive oxygen species (ROS) content and decreased mitochondrial membrane potential in L8824 cells, which induced an up-regulation of the expression of mitophagy-related indicators (PINK1, Parkin, Beclin1, LC3B, and ATG5) and a down-regulation of P62. An up-regulation of the expression of the ferroptosis-related indicators TFR1 and COX-2, and GPX4 and FTH expression was down-regulated. In addition, there was a decrease in the expression of IL-2 and IFN-γ and an increase in the expression of inflammatory cytokines such as TNF-α, IL-1β, and IL-6 after exposure to MEHP. RSV activates the Nrf2 pathway and effectively alleviates MEHP-induced mitophagy, ferroptosis, and immunologic dysfunction of L8824 cells.

1. Introduction

DEHP is an extensively utilized plasticizer in food processing, industrial, medicinal, and other industries (Fu et al., 2023). The primary metabolite of DEHP is MEHP, which has a high level of toxicity (Zhang et al., 2022a). DEHP in plastic products can be released into the environment and seriously pollute water resources and the environment (Dueñas-Moreno et al., 2023). In a wastewater study in Poland, the concentration of DEHP in wastewater samples was up to 143 mg/L (Kotowska et al., 2020). In the environment, DEHP can be converted to MEHP by abiotic and biological processes. One study examined surface water samples collected in the upper, middle, and lower reaches of the Dongjiang River Basin and found that DEHP accounted for 91% of all detected phthalates (PAEs) and MEHP accounted for 73% of all detected PAE monoesters (Li et al., 2024). Another study found that when plastics enter a water environment, the plastic surface inevitably forms a biofilm, and although the presence of a surface biofilm causes the concentration of DEHP in water to decrease by 0.8–11.6 times, the concentration of MEHP in water increases by 2.3–57.3 times (Zhao et al., 2024). DEHP is immediately hydrolyzed to the more stable MEHP upon entry into the biological organism (Chen et al., 2022). Studies have reported that MEHP remains in human sweat, blood, hair, and breast milk (Zhang et al., 2021). More and more studies have confirmed the severe damage caused by MEHP to biological organisms. MEHP can penetrate

☆ All authors have read the manuscript and agreed to submit it in its current form for consideration for publication in the Journal.

* Corresponding author. College of Veterinary Medicine, Northeast Agricultural University, Harbin, 150030, China.
** Corresponding author. College of Veterinary Medicine, Northeast Agricultural University, Harbin, 150030, China.
E-mail addresses: tongxu@neau.edu.cn (T. Xu), linhongjin@neau.edu.cn (H. Lin).

https://doi.org/10.1016/j.jenvman.2024.123235
Received 7 August 2024; Received in revised form 22 October 2024; Accepted 1 November 2024
Available online 6 November 2024

the blood-testis barrier and damage the male reproductive system (Hong et al., 2023a, 2023b). MEHP is more likely than DEHP to cause endothelial cell dysfunction in the brain and compromise the integrity of the blood-brain barrier (Kim et al., 2023). MEHP also induces thyroid toxicity by causing endoplasmic reticulum stress (Xu et al., 2022a). In addition, MEHP can induce oxidative stress, causing neurotoxicity (Liu et al., 2023a). It is worth noting that the liver is the most significant metabolic organ of the animal organism and has the function of detoxification. MEHP can cause lipid metabolism disorder and liver fibrosis from oxidative damage to hepatocytes in rats (Zhang et al., 2022b, 2023a). In addition, MEHP induces hepatic injury in pregnant mice via lipid peroxidation and iron accumulation (Zhang et al., 2022c). As a result, many researchers have initiated studies on MEHP detoxification drugs. For example, Pinar Erkekoglu et al. found that selenium supplementation attenuated MEHP-induced LNCaP cytogenetic toxicity by alleviating oxidative stress (Erkekoğlu et al., 2010). Sorour Ashari et al. demonstrated that quercetin can reduce MEHP-induced kidney damage by modulating the NF-κB signaling pathway (Ashari et al., 2022).

The regulation of oxidation and antioxidants is essential for maintaining normal physiological functions and resisting diseases (Li et al., 2023a; Gao et al., 2022a; Xu et al., 2022b). Oxidative stress results from an imbalance between oxidative and antioxidant processes caused by excess ROS (Lv et al., 2023; Wang et al., 2023a, 2024; Miao et al., 2023; Sun et al., 2024a; Lei et al., 2024). The Nrf2 pathway is essential for preserving cellular homeostasis and regulating oxidative stress (Huang et al., 2023; Hou et al., 2022; Li et al., 2023b). Normal conditions result in the presence of Nrf2 as the Keap1-Nrf2 complex in the cytoplasm. When external stimuli cause oxidative stress, Keap1 separates from Nrf2, and Nrf2 enters the nucleus to promote the synthesis of downstream antioxidant enzymes such as HO-1 and NQO1 (Xing et al., 2023; Lim et al., 2021). Mitochondria are essential sites of cellular metabolism and targets of ROS action (Kasai et al., 2023). The increase in oxidative stress impaired mitochondrial function and induced mitophagy (Wang et al., 2023b). It has been shown that bisphenol S affects the Nrf2 antioxidant pathway and promotes apoptosis and mitophagy in mouse osteoblasts by inducing mitochondrial ROS production (Shan et al., 2023). Furthermore, co-exposure to cadmium and polystyrene nano plastics exacerbated oxidative stress and excessive mitophagy in mouse kidneys by inhibiting the Nrf2 antioxidant pathway (Qiu et al., 2023). A large number of studies have shown that oxidative stress can induce ferroptosis (Zhu et al., 2023a; Dong et al., 2023; Yang et al., 2024). Moreover, ferroptosis is strongly associated with the Nrf2 pathway (Wang et al., 2023c). According to recent research, vitexin activates the Nrf2 pathway in renal tubular epithelial cells, inhibiting ferroptosis and mitigating chronic kidney disease (Song et al., 2023). By blocking ferroptosis via the Nrf2 signaling pathway, caffeine reduces the effects of cerebral ischemia in rats (Li et al., 2023c). Furthermore, oxidative stress can lead to immune dysfunction (Zheng et al., 2019; Cai et al., 2023). At the same time, the Nrf2 pathway is also involved in immune regulation. Nrf2 is considered to be an important regulator of innate immunity (Zhu et al., 2023b). For example, co-exposure of abamectin and imidacloprid induced immune dysfunction in carp epithelial cells by influencing the Keap1/Nrf2/TXNIP axis (Liu et al., 2023b); Dendritic cells are shielded against immunological dysfunction caused by lipopolysaccharides by astaxanthin-induced Nrf2/HO-1 axis activation (Yin et al., 2021).

RSV is a natural polyphenol organic compound that comes from many dietary fruits such as grapes and mulberries (Griñán-Ferré et al., 2021). RSV has the properties of resisting oxidative stress and inflammation through the Nrf2 pathway (Shahcheraghi et al., 2023). Studies have shown that RSV can protect cardiomyocytes by reducing mitophagy induced by zinc deficiency (Wang et al., 2023d). RSV also prevents ischemia-reperfusion injury in the myocardium by attenuating oxidative stress and ferroptosis (Li et al., 2022a). In addition, RSV significantly enhanced immune function in immunosuppressed mice (Lai et al., 2016). However, uncertainty exists regarding RSV's potential antagonistic effects on the MEHP-induced immunological dysfunction, ferroptosis, and mitophagy of L8824 cells. Thus, to ascertain the experimental concentration of MEHP and the ideal antagonistic concentration of RSV, we employed the CCK-8 kit to measure the vitality of L8824 cells treated with RSV and/or MEHP. Subsequently, a DCFH-DA probe and an oxidative stress kit were used to determine each group's degree of oxidative stress. Finally, the related indexes of the Nrf2 pathway, mitophagy, ferroptosis, and immune function were examined by molecular docking, immunofluorescence, JC-1 staining, MDC staining, Western blot, and RT-PCR. This work aimed to explore the effect of RSV on MEHP-induced cell damage and its relationship with the Nrf2 pathway, to provide a foundation for developing MEHP detoxification drugs, and to provide a scientific foundation for aquatic organisms to avoid the threat of MEHP.

2. Materials and methods

2.1. Experimental medicines

Mono(2-ethylhexyl) phthalate (purity ≥98%, Yuan ye, China) chemical formula $C_{16}H_{22}O_4$ (CAS:4376-20-9) is the main metabolite of DEHP. Resveratrol (purity ≥99%, Macklin, China) with chemical formula $C_{14}H_{12}O_3$(CAS:501-36-0) is a natural antioxidant found in plants. ML385(purity ≥99%, MedChemExpress, USA) is a commonly used Nrf2 inhibitor (Cat.No:HY-100523). MEHP, RSV, and ML385 were dissolved with DMSO (purity ≥99%, Biotope, China).

2.2. Cell culture and treatment

The culture method of grass carp hepatocytes (L8824 cells) was referred to in our previous study (Gao et al., 2022b). The CCK-8 kit (Meilun Bio, China) was utilized in this investigation to assess the toxicity of RSV and/or MEHP to L8824 cells. L8824 cells were exposed to MEHP (0, 2, 4, 8, 16, 32, 64, 128, 256, 512, 1024 μM), RSV (0, 0.25, 0.5, 1, 2, 4, 8, 16, 32, 64, 100 μM) and MEHP (85 μM) + RSV (0、0.25、0.5、1、2、4、8、16、32、64 μM). According to the experimental results of CCK8, four experimental groups were created: Control group, RSV (2 μM) group, MEHP (85 μM) group, RSV (2 μM) + MEHP (85 μM) group.

2.3. Detection of oxidative stress level

The DCFH-DA fluorescent probe was employed in this investigation to detect the accumulation of ROS in each cell group. After inoculating each group's cells in 6-well plates, the working solution was set up with a probe and PBS ratio of 1:1000. The medium in the plates was discarded. After three PBS washes, each well was filled with 1 mL of the working solution. After 30 min of light-protected incubation, each group was examined under a fluorescence microscope.

To ascertain each group's cells' antioxidant capacity, an oxidative stress kit (A001-1-2, A007-1-1, A005-1-2, A015-1-2, A003-1-2, Nanjing Jiancheng Bioengineering Institute, China) was utilized. Each group's cells were pretreated by the oxidative stress kit's instructions, and Superoxide dismutase (SOD), Catalase (CAT), Glutathione peroxidase (GSH-Px), Total antioxidant capacity (T-AOC), and Malondialdehyde (MDA) were detected in the supernatant that was collected following treatment.

2.4. Molecular docking

The binding energies of RSV and Keap1 were calculated by molecular docking, and the 3D structures of Keap1 and RSV were obtained in the same way as in our previous study (Gao et al., 2022a). The software used for molecular docking was Auto Dock Vina. Finally, PyMol 2.6.0 was utilized to screen the optimal binding modes of RSV and Keap1, in which the first binding result was optimal.

2.5. Detection of mitochondrial membrane potential (ΔΨm)

The Mitochondrial Membrane Potential Kit (JC-1, Beyotime, China) is a kit that uses JC-1 as a probe to detect changes in the cellular mitochondrial membrane potential quickly and sensitively. 5 μL of JC-1 probe was added to each 1 mL of JC-1 buffer to configure the JC-1 working solution. The cells of each group were inoculated in 6-well plates, and after discarding the medium, 1 mL of JC-1 working solution was added to each well, and the cells were left to incubate for 20 min without exposure to light. Finally, the JC-1 working fluid was discarded, and 1 mL of medium was added to each well. The changes in mitochondrial membrane potential in each group's cells were observed under the microscope.

2.6. MDC dyeing

Autophagy Staining Detection Kit (MDC, Beyotime, China) is one of the most commonly used kits to detect autophagy. An appropriate amount of MDC probe was taken and diluted into MDC stain solution with Assay Buffer at a ratio of 1:1000. Discard each group of cells' culture medium, wash with PBS three times, add 1 mL of MDC staining solution to each well, and incubate for 30 min without exposure to light. Ultimately, after discarding the MDC staining solution and cleaning each well twice with Assay Buffer, each well was given 1 mL of Assay Buffer, and the formation of autophagosomes in each group was observed under a fluorescence microscope.

2.7. Immunofluorescence

The cells of each group were inoculated into 12-well plates, 1 mL 4% paraformaldehyde was added to each well, and the cells were placed in a shaking bed at 4 °C overnight. The fixed liquid was discarded, the washing liquid was washed three times, and a blocking solution was used to block the cells for 1 h. Discard the blocking solution and incubate at 4 °C overnight with diluted primary antibody (GPX4, Abmart, Dilution ratio:1:200). After recovering the primary antibody, add the diluted secondary antibody (Dylight 488 goat anti rabbit IgG, Biodragon, Dilution ratio:1:1000). Remove from light and incubate for 1 h at room temperature. The secondary antibody was recovered, and another target primary antibody (FTH, ABclonal Biotechnology, Dilution ratio:1:200) was added. Remove from light and incubate for 2 h at 37 °C. After the primary antibody was recovered, another secondary antibody (Dylight 594 goat anti rabbit IgG, Biodragon, Dilution ratio:1:1000) was added and incubated in a room. The secondary antibodies were recovered, washed three times in washing solution, and after adding 500 μL of DAPI nuclear dye to each well, the wells were left in the dark for 15 min. Ultimately, following three washings with a washing solution and the addition of an anti-fluorescence quencher, each group's fluorescence intensity was examined under a fluorescence microscope.

2.8. Real-time quantitative PCR (RT-PCR) analysis

Using the Trizol method (Thermo Scientific, USA), total RNA was isolated from each treatment group in this investigation. The extraction of RNA by Triol mainly includes the following steps: First, the cell is lysed by Triol reagent; Then, chloroform is added for phase separation. The upper water phase was absorbed, and isopropyl alcohol was added to precipitate RNA. After that, RNA precipitation was washed with 75% DEPC alcohol. Finally, the RNA precipitate was dissolved in the DEPC water, producing high-quality RNA. A reverse transcription kit (TransGen, China) was then used to convert the extracted total RNA into cDNA. The target genes' mRNA levels were found using the Light Cycler ® 480 II apparatus. The $2^{-\Delta\Delta Ct}$ method was used to calculate relative mRNA expression. β-actin was used as the internal reference gene. Table 1 lists the primer sequences that were used in this investigation.

2.9. Protein extraction and Western blot analysis

The cells in each group were inoculated in a 6-well plate for the extraction of total cell protein, and the protein lysate was prepared at a ratio of 1 mL RIPA (Beyotime, China) to 10 μL PMSF (Beyotime, China). Each group was added 1 mL of protein lysate, scraped off the cells, and then the mixture was placed in a 1.5 mL centrifuge tube for ultrasound using an ultrasonic cell crusher. Then, centrifuge at 4 °C for 12,000 r/min for 15 min, absorb 700 μL of liquid in the middle layer, add 175 μL of SDS, shake and mix, heat for 15 min at 100 °C in a metal bath, and store at −80 °C.

The proteins were transferred to the NC membrane after being isolated by SDS-PAGE. 5% skim milk was used as the blocking solution, blocked at 37 °C for 2 h, and incubated overnight with diluted primary antibody. Finally, they were scanned using the Azure Imaging Biosystem C300 after being incubated with secondary antibodies for 2 h. Table 2 displays the primary antibodies that were employed in this research.

2.10. Data statistics and analysis

The data analysis software used in this study was GraphPad Prism 9.0. The T-test was employed to examine the variations among the

Table 1
The primer sequences utilized in this assay.

Genes	Upstream primer (5′–3′)	Downstream primer (5′–3′)
Keap1	ACAAGCCCACCAAAGTCATTCC	TATCCGCCAGCCGTGTAGATG
Nrf2	CGTGAGCAGGAGGAGGAGAAG	TTTGTTGTGTTGGTTTGCGTTAGC
HO-1	CAGCATCCCAAAGTCAATCAAGAAC	ATTCCCACACCTAACGCAAACTG
NQO1	CGACGAGAAATGGCACAGAAGAC	GAAGTTCATAGCATAGAGATCCGACAC
PINK1	GAGATCCTTCCTTGCCAACATAGAC	ACTGCCATTGCTCTTGTCCATAC
Parkin	AGCGGAGGAGTGTGTTCTTCAG	AAACCCACAGCCAAGTCCATTTC
P62	GACCAAGGCAGTGATGAGGAATG	TGTGCTGGAGGCGGTACTTAG
Beclin1	CGGCTCCATTAGTGACAGTTACAG	GTGCTCTCAGTTGACATCATCCTC
LC3B	CTTCCTGCTTGTCAACGGTCAC	CAAATGTCTCCTGGGATGCGTAG
ATG5	AGCCAAAGAGATTCCAGGTTATGATTC	GATGCTGATGTGGAGGAAGTTGTC
GPX4	CGCCAAGTCTTACAACGCAGAG	TCCTTCAGCCACTTCCACAGAG
FTH	CAGGACGTGAAGAAACCAGAGAAGG	TGAGGGTCGTTGTGCTGAGAGG
TFR1	AATGGATGGAACAGAACAAGGACAC	CACAGAAGACAGCCAGCACAAC
COX-2	AGACTACGAAGATTTAGGCTTTGACTC	GATACTAGGACACGAACTGGTGATTC
TNF-α	GTGATGGTGCCGAGGAGGAAG	CTCTGAGACTTGTTGAGCGTGAAG
IL-1β	GTGCTGATTCTGATGAGATGGACTG	CAATGATGATGTTCACCACTTGCTTC
IL-2	TTCAGGAGGATTGTTTGTCTTCAGC	CCTTGTTCAGTCCTTCGTAGATCATC
IFN-γ	AGTCCAGAAATCCGCCTCAGAG	TTCCATCGTGCTTCAACTCCATAG
IL-6	AGGTGAGTGAAGGACAGATGGATC	TGACGCTGGTGAAGTTGAACAAG
β-Actin	CGTGCTGTCTTCCCATCCATCG	CTGAGCCTCGTCACCAACATAGC

Table 2
The antibodies utilized in this assay.

Genes	Dilution ratio	Manufacturer	Cat. No
Keap1	1:1000	Wan lei, Shenyang, China	WL03285
Nrf2	1:500	Wan lei, Shenyang, China	WL02135
HO-1	1:1000	Wan lei, Shenyang, China	WL02400
NQO1	1:500	Wan lei, Shenyang, China	WL04860
PINK1	1:500	ABclonal Biotechnology	A24745
Parkin	1:500	Wan lei, Shenyang, China	WL02512
P62	1:500	Wan lei, Shenyang, China	WL02385
Beclin1	1:1000	Wan lei, Shenyang, China	WL02508
LC3B	1:1000	Wan lei, Shenyang, China	WL01506
ATG5	1:1000	Wan lei, Shenyang, China	WL02411
GPX4	1:500	Wan lei, Shenyang, China	WL05406
FTH	1:500	Wan lei, Shenyang, China	WL05360
TFR1	1:500	Wan lei, Shenyang, China	WL03500
COX-2	1:1000	Wan lei, Shenyang, China	WL01750
TNF-α	1:1000	ABclonal Biotechnology	A24214
IL-1β	1:500	Wan lei, Shenyang, China	WL00891
IL-2	1:1500	Wan lei, Shenyang, China	WL00693
IFN-γ	1:1500	Wan lei, Shenyang, China	WL02440
IL-6	1:1000	Wan lei, Shenyang, China	WL02841
β-Actin	1:10,000	ABclonal Biotechnology	AC026

groups. Every experiment was conducted thrice, and the results were displayed as mean ± standard deviation. The superscript letters between two groups are ns for $p > 0.05$, * for $p < 0.05$, ** for $p < 0.01$, *** for $p < 0.001$, and **** for $p < 0.0001$.

3. Experimental results

3.1. RSV reduces the decline in L8824 cell viability brought on by exposure to MEHP

Using the CCK-8 kit, the impact of exposure to RSV and/or MEHP on the viability of L8824 cells was investigated to be able to establish the experimental concentrations of RSV and MEHP. As shown in Fig. 1A, L8824's cell viability declined dose-dependently following MEHP treatment, with a median inhibitory concentration of 331.9 μM (95% confidence interval 273.8–410.3). When RSV concentration was less than 8 μM, the viability of L8824 cells was not affected. When RSV concentration was greater than 8 μM, the viability of L8824 cells was decreased in a dose-dependent manner (Fig. 1B). In order to determine the optimal concentration of RSV against MEHP, L8824 cells were treated with 85 μM MEHP (cell survival rate was 74.592%) and various concentrations of RSV, and the detoxification impact of MEHP was most pronounced at RSV concentration of 2 μM (Fig. 1C). Therefore, the experimental concentrations of MEHP and RSV were finally determined to be 85 μM and 2 μM, respectively.

3.2. RSV reduces the oxidative stress that exposure to MEHP causes in L8824 cells

ROS fluorescent probes were used to measure the impact of RSV and/or MEHP exposure on the level of oxidative stress in L8824 cells. The production of ROS observed by fluorescence microscopy is depicted in Fig. 2A. Fig. 2A was quantized using image j software, yielding Fig. 2B. According to the experimental result, the MEHP group generated considerably more ROS than the Control and RSV groups ($p < 0.05$). Conversely, the RSV + MEHP group generated significantly less ROS than the MEHP group. Next, we performed oxidative stress kits (Fig. 2C). The findings demonstrated that whereas the MEHP group had much greater levels of MDA than the Control group, the activities of CAT, GSH-Px, SOD, and the level of T-AOC in the MEHP group were significantly decreased. In comparison to the MEHP group, there was a significant increase in the activities of CAT, GSH-Px, SOD and the levels of T-AOC and a significant decrease in the levels of MDA after receiving MEHP and RSV co-treatment. The experimental results showed that RSV effectively reduced the oxidative stress that MEHP exposure had caused in L8824 cells.

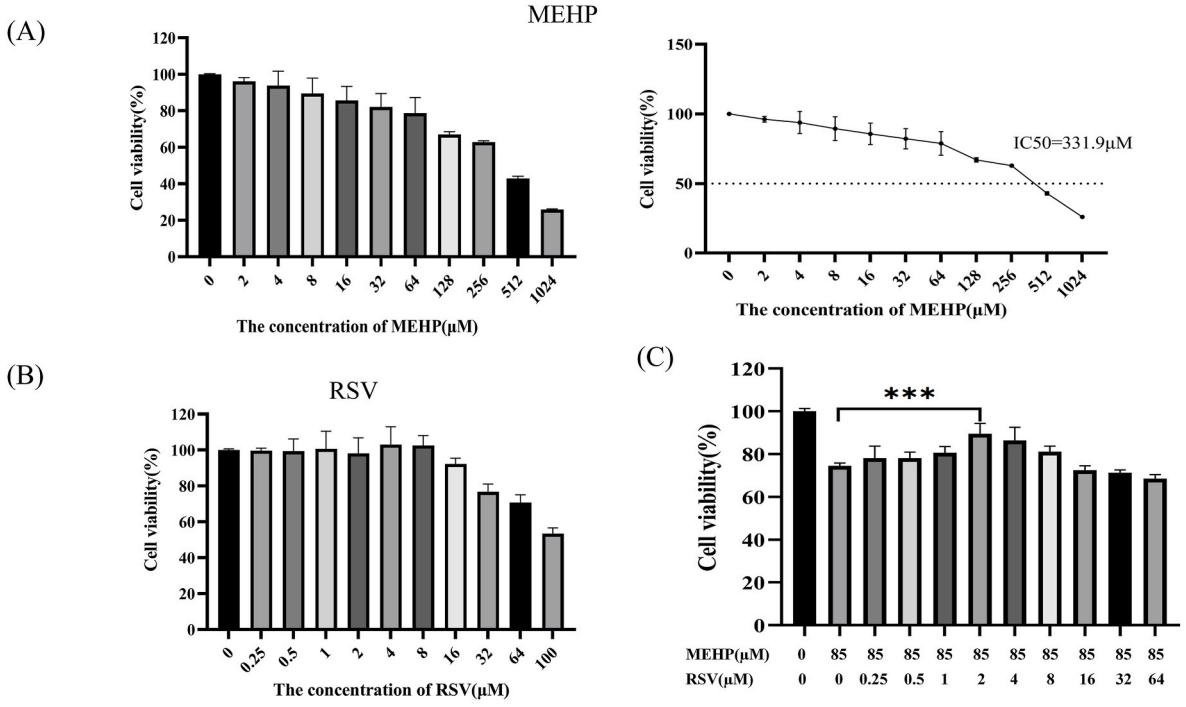

Fig. 1. RSV mitigated MEHP-induced decline in L8824 cell viability. (A) Changes in cell viability of L8824 cells treated with different concentrations of MEHP. (B) Changes in cell viability of L8824 cells treated with different concentrations of RSV. (C) The effects of 85 μM MEHP and different concentrations of RSV on the viability of L8824 cells. All data were expressed as mean ± standard deviation. The superscript letters between the two groups are ns for $p > 0.05$, * for $p < 0.05$, ** for $p < 0.01$, *** for $p < 0.001$, and **** for $p < 0.0001$, the same below.

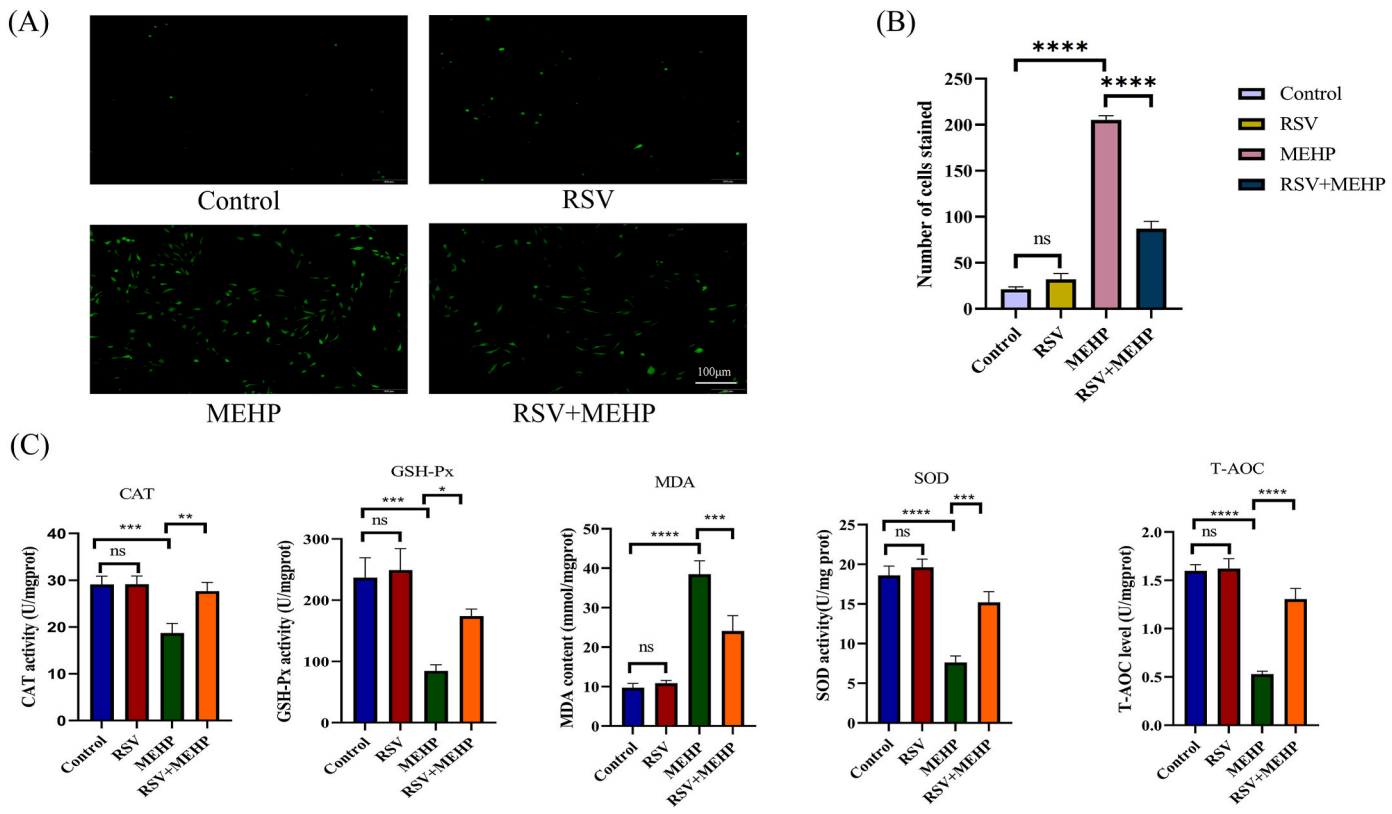

Fig. 2. RSV alleviates oxidative stress in L8824 cells induced by MEHP exposure. The scales in Fig. 2A are all 100 μm. (A) The production of ROS in each group was observed under the fluorescence microscope. (B) Quantification of Fig. 2A. (C) Oxidative stress kit: CAT, GSH-Px, MDA, SOD, T-AOC detection results data.

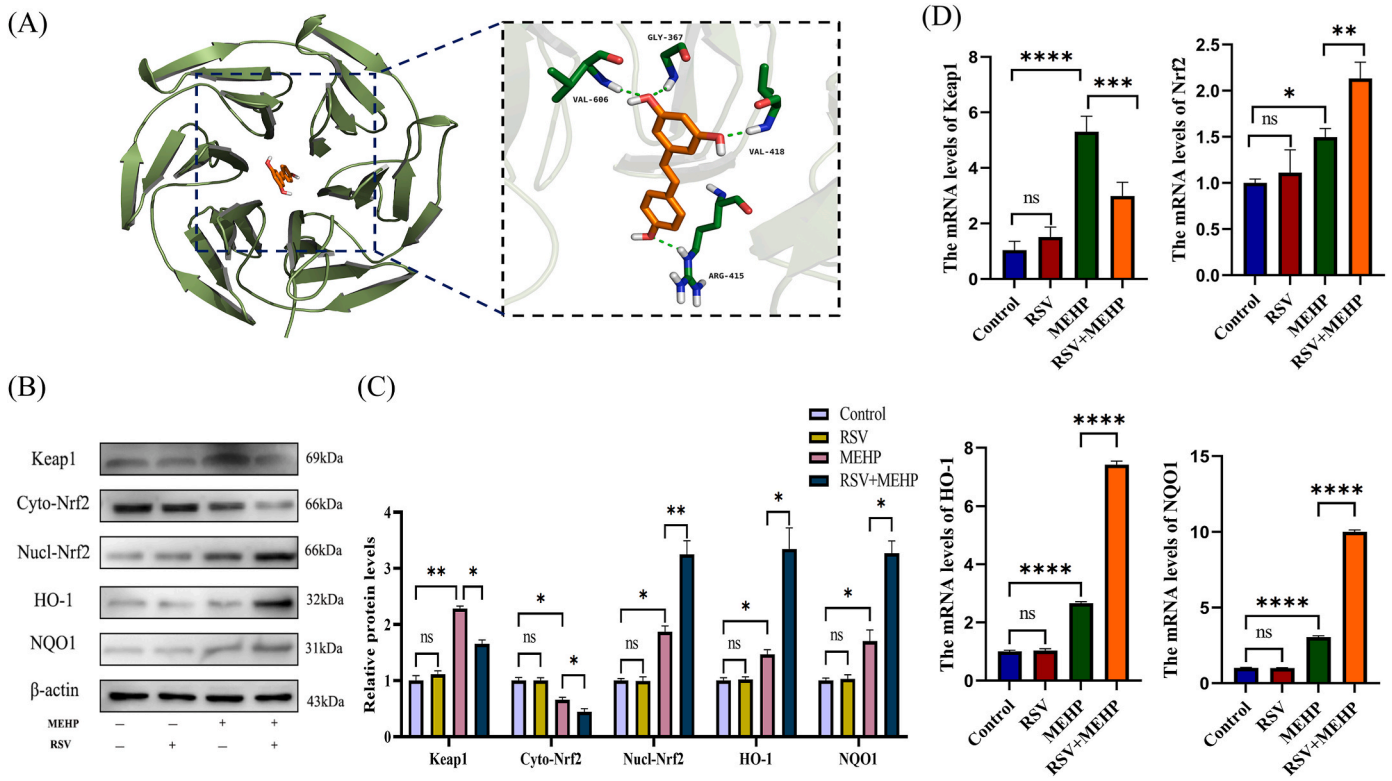

Fig. 3. Effects of RSV and/or MEHP exposure on the Keap1/Nrf2 pathway. (A) Molecular docking of RSV and Keap1. The diagram of the molecular binding sites of RSV and Keap1 is shown in the right window. (B) Expression of the Nrf2 pathway-related proteins in different treatment groups. (C) Quantification of Fig. 3B. (D) Expression of the Nrf2 pathway-related mRNA in different treatment groups. Data are expressed as mean ± standard deviation.

3.3. RSV regulates the Nrf2 pathway to alleviate the damage of L8824 cells induced by MEHP

Using molecular docking, Western blot, and RT-PCR, the effects of RSV and/or MEHP exposure on the Nrf2 pathway were investigated in this work. Fig. 3A shows the molecular docking of RSV and Keap1. The binding energy is −8.3 kcal/mol, and the two have strong binding ability with four binding sites. Glycine 367 (GLY-367), Valine 606(VAL-606), Valine 418(VAL-418), arginine 415 (ARG-415). Therefore, it is hypothesized that RSV may bind Keap1 protein either directly or indirectly to function. Next, we examined each group's expression of proteins associated with the Nrf2 pathway (Fig. 3B). Keap1 expression in the MEHP group was significantly higher than that in the control group ($p < 0.05$). Keap1 expression in the RSV + MEHP group was significantly lower than that in the MEHP group ($p < 0.05$). Regarding the expression of Nrf2 protein, the experimental results showed a considerable decline in intracellular Nrf2 expression and a considerable increase in nuclear expression in the MEHP group compared to the Control group, with a more significant decrease in intracellular Nrf2 expression and a more significant increase in nuclear expression in the RSV + MEHP group ($p < 0.05$). Moreover, with the transfer of Nrf2 into the nucleus, the protein expressions of downstream antioxidant enzymes HO-1 and NQO1 were significantly enhanced. Compared with the control group, the protein expressions of HO-1 and NQO1 in the MEHP group were enhanced to a certain extent, and the protein expressions of HO-1 and NQO1 in the RSV + MEHP group were the most significantly enhanced. Fig. 3D displays the mRNA associated with the Nrf2 pathway expressed in each treatment group. This mRNA expression trend aligns with that of the protein expression. These findings demonstrated that RSV could control the Nrf2 pathway to lessen the adverse impacts of MEHP on L8824 cells.

3.4. RSV alleviation mitophagy induced by MEHP exposure in L8824 cells

Firstly, using a mitochondrial membrane potential kit, the variations in each group's mitochondrial membrane potential were identified (Fig. 4A). The findings demonstrated that the MEHP group's green fluorescence was increased while its red fluorescence was dramatically diminished when compared to the Control group, suggesting a drop in the potential of the mitochondrial membrane. Compared with the MEHP group, the mitochondrial membrane potential in the RSV + MEHP group recovered significantly. Fig. 4C shows the generation of autophagosomes in each group as observed under fluorescence microscopy. The MEHP group had significantly more autophagosomes than the Control group, while the RSV + MEHP group had significantly fewer autophagosomes than the MEHP group. The expression of proteins linked to mitophagy in each group was next investigated (Fig. 4E). The outcomes demonstrated that the MEHP group's protein expressions of PINK1, Parkin, Beclin1, LC3B, and ATG5 were considerably greater than those of the Control group ($p < 0.05$). Conversely, P62's protein expression was considerably lower ($p < 0.05$). The RSV + MEHP group showed considerably lower protein expressions of PINK1, Parkin, Beclin1, LC3B, and ATG5 than the MEHP group but significantly higher levels of P62 ($p < 0.05$). Moreover, the expression trend of mitophagy-related mRNA was consistent with that of protein (Fig. 4G). These findings showed that RSV could prevent the onset of mitophagy in L8824 cells, whereas MEHP increased it.

3.5. RSV alleviates ferroptosis of L8824 cells induced by MEHP exposure

To assess the occurrence of ferroptosis in each group, the ferroptosis markers GPX4 and FTH were detected by immunofluorescence double staining (Fig. 5A). The figure illustrates that the fluorescence intensity of GPX4 and FTH in the MEHP group was much lower than in the Control group. In contrast, the RSV + MEHP group's fluorescence intensity was considerably greater than in the MEHP group. In conclusion, MEHP can induce ferroptosis in L8824 cells, while RSV can alleviate MEHP-induced ferroptosis in L8824 cells. To validate this idea further, we examined ferroptosis-related proteins in each group. As demonstrated in Fig. 5D, the MEHP group's protein expressions of TFR1 and COX-2 were considerably raised compared with the Control group ($p < 0.05$), while the protein expressions of GPX4 and FTH were dramatically lowered ($p < 0.05$). In the RSV + MEHP group, there was a substantial rise in the protein expressions of GPX4 and FTH compared to the MEHP group ($p < 0.05$) and a significant decrease in the protein expressions of TFR1 and COX-2 ($p < 0.05$). The expression of ferroptosis-associated mRNAs is consistent with the trend of protein expression, as shown in Fig. 5F.

3.6. RSV alleviates the immunological dysfunction brought on by exposure to MEHP in L8824 cells

The impact of RSV and/or MEHP exposure on the immunological function of L8824 cells was finally assessed by investigating the mRNA and protein expression of TNF-α, IL-1β, IL-2, IFN-γ, and IL-6. The findings demonstrated that the MEHP group's protein expressions of TNF-α, IL-1β, and IL-6 were considerably greater in comparison to the Control group ($p < 0.05$), while the protein expressions of IL-2 and IFN-γ were considerably lower ($p < 0.05$). In contrast to the MEHP group, protein expressions of TNF-α, IL-1β, and IL-6 in the RSV + MEHP group were considerably declined ($p < 0.05$), and the protein expressions of IL-2 and IFN-γ were considerably increased ($p < 0.05$)(Fig. 6A). Fig. 6B shows that the expression of immunological dysfunction mRNAs is consistent with the trend of protein expression. These findings implied that RSV reduced the harmful impact caused by exposure to MEHP on the immune systems of L8824 cells.

3.7. RSV alleviates mitophagy, ferroptosis, and immune dysfunction of L8824 cells induced by MEHP by regulating the Nrf2 pathway

We added ML385(Nrf2 inhibitor, 5 μM) to verify further that RSV alleviates a series of cell damage induced by MEHP by regulating the Nrf2 pathway. Firstly, we detected the protein expression of Nrf2. The results showed that compared with the MEHP group, Nucl-Nrf2 protein expression in the MEHP + ML385 group was significantly decreased ($p < 0.05$). Compared with the RSV + MEHP group, the expression level of Nucl-Nrf2 protein in the RSV + MEHP + ML385 group was also significantly decreased ($p < 0.05$). This indicated that ML385 significantly inhibited the activation of Nrf2, and the expression of antioxidant enzymes HO-1 and NQO1 decreased significantly with the inhibition of Nrf2 (Fig. 7A). Fig. 7B shows the expression of mRNA associated with the Nrf2 pathway and the trend is consistent with the proteins. Subsequently, ROS content in each group was detected (Fig. 7C). The results showed that inhibition of Nrf2 increased the oxidative stress induced by MEHP and reversed the antioxidant effect of RSV. Fig. 7E and G showed the changes in mitochondrial membrane potential and autophagosome formation of each group under fluorescence microscopy. Compared with the RSV + MEHP group, the mitochondrial membrane potential of the RSV + MEHP + ML385 group decreased significantly, and autophagosome formation increased significantly ($p < 0.05$). This suggests that inhibition of the Nrf2 pathway reversed the inhibitory effect of RSV on mitophagy induced by MEHP in L8824 cells. We further verified this idea by examining the expression of mitophagy-associated proteins (Fig. 7I) and genes (Fig. 7J). Next, we examined the occurrence of ferroptosis in each group (Fig. 7K). As shown in the figure, compared with the RSV + MEHP group, the fluorescence intensity of GPX4 and FTH in the RSV + MEHP + ML385 group was significantly decreased ($p < 0.05$). Combined with the detection of ferroptosis-related protein (Fig. 7L) and mRNA (Fig. 7M) expression, we found that inhibition of the Nrf2 antioxidant pathway reversed the alleviating effect of RSV on ferroptosis of L8824 cells induced by MEHP. Finally, the protein (Fig. 7N) and the mRNA (Fig. 7O) expressions of TNF-α, IL-1β, IL-2, IFN-γ, and IL-

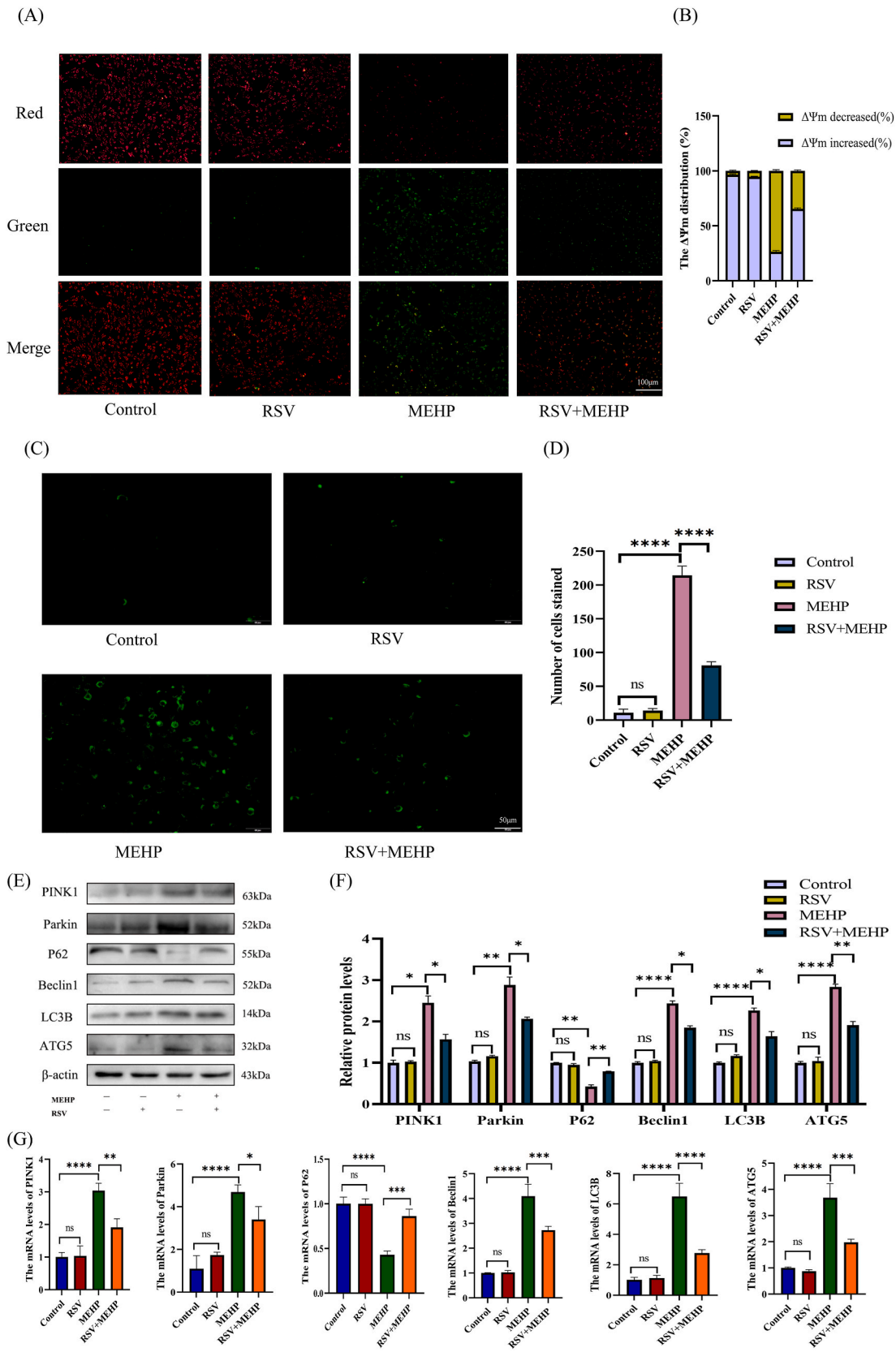

Fig. 4. RSV alleviates mitophagy in L8824 cells induced by MEHP exposure. (A) The changes in mitochondrial membrane potential in each group were observed under the fluorescence microscope after JC-1 staining. The scale in Fig. 4A was 100 μm for all groups. (B) Quantification of Fig. 4A. (C) The formation of autophagosomes in each group was observed under the fluorescence microscope after MDC staining, and the scale in Fig. 4C was all 50 μm. (D) Quantification of Fig. 4C. (E) Expression of mitophagy-associated proteins in different treatment groups. (F) Quantification of Fig. 4E. (G) Expression of mitophagy-related mRNAs in different treatment groups. Data are expressed as mean ± standard deviation.

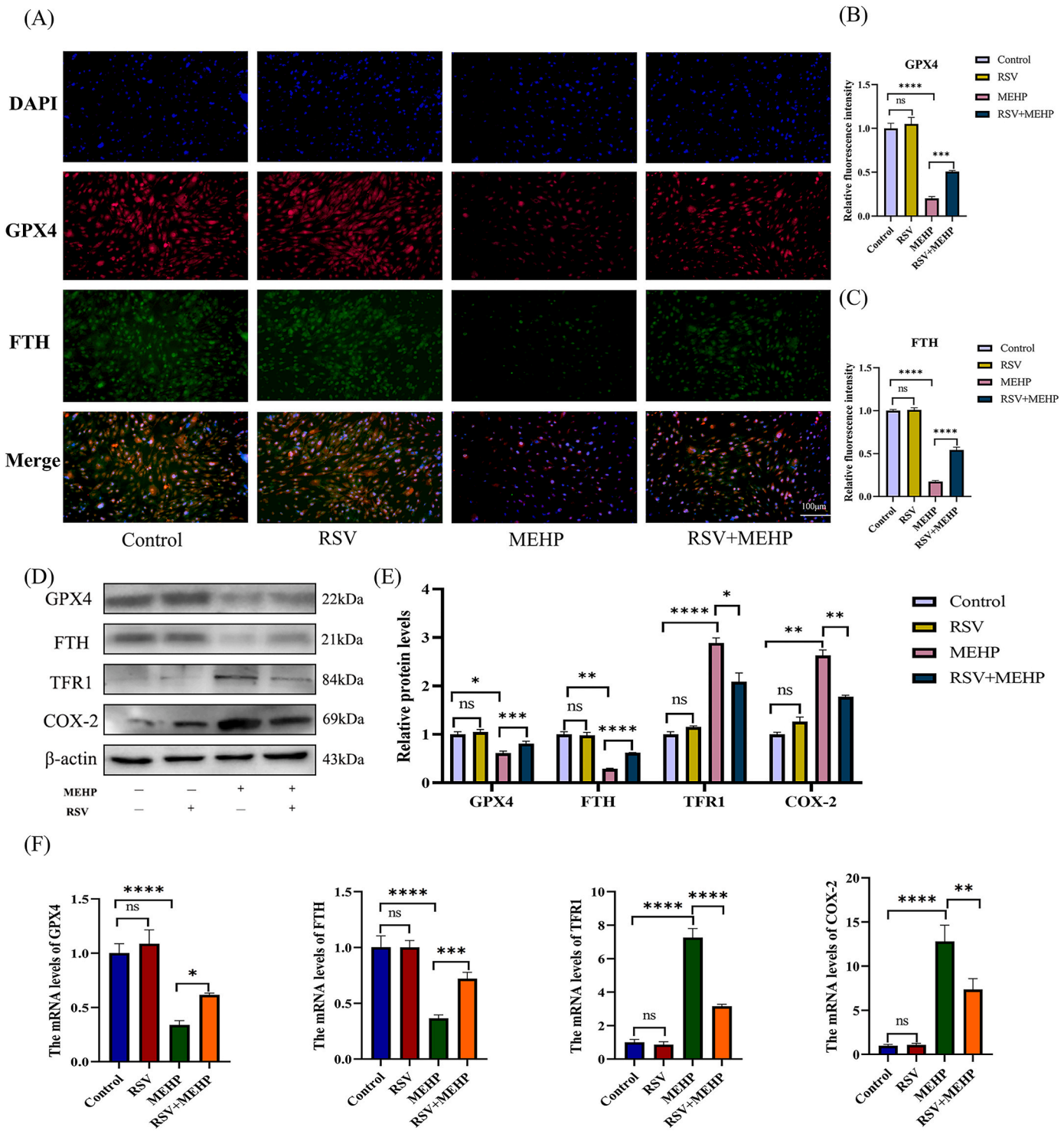

Fig. 5. RSV alleviates ferroptosis in L8824 cells induced by MEHP exposure. (A) Immunofluorescence double staining of GPX4 and FTH. The scales in Fig. 5A are all 100 μm. (B) Quantification of GPX4 fluorescence intensity. (C) Quantification of FTH fluorescence intensity. (D) Expression of ferroptosis-related proteins in different treatment groups. (E) Quantification of Fig. 5D. (F) Expression of ferroptosis-related mRNA in different treatment groups.

6 were detected. Compared with the RSV + MEHP group, the protein and the mRNA expressions of TNF-α, IL-1β, and IL-6 were significantly increased *($p < 0.05$)*, the protein and the mRNA expressions of IL-2 and IFN-γ were significantly decreased *($p < 0.05$)* in the RSV + MEHP + ML385 group. These results indicated that inhibition of the Nrf2 antioxidant pathway reversed the remission effect of RSV on the immune dysfunction of L8824 cells induced by MEHP. The above results indicate that RSV alleviates mitophagy, ferroptosis, and immune dysfunction of L8824 cells induced by MEHP by regulating the Nrf2 pathway.

4. Discussion

MEHP is a highly toxic environmental endocrine disruptor as a hydrolysis product of DEHP (Li et al., 2023d). In a study utilizing 5-amino fluorescein-modified MEHP (MEHP-AF) on behalf of MEHP to study its toxicokinetics, it was concluded that the liver is one of the main toxic

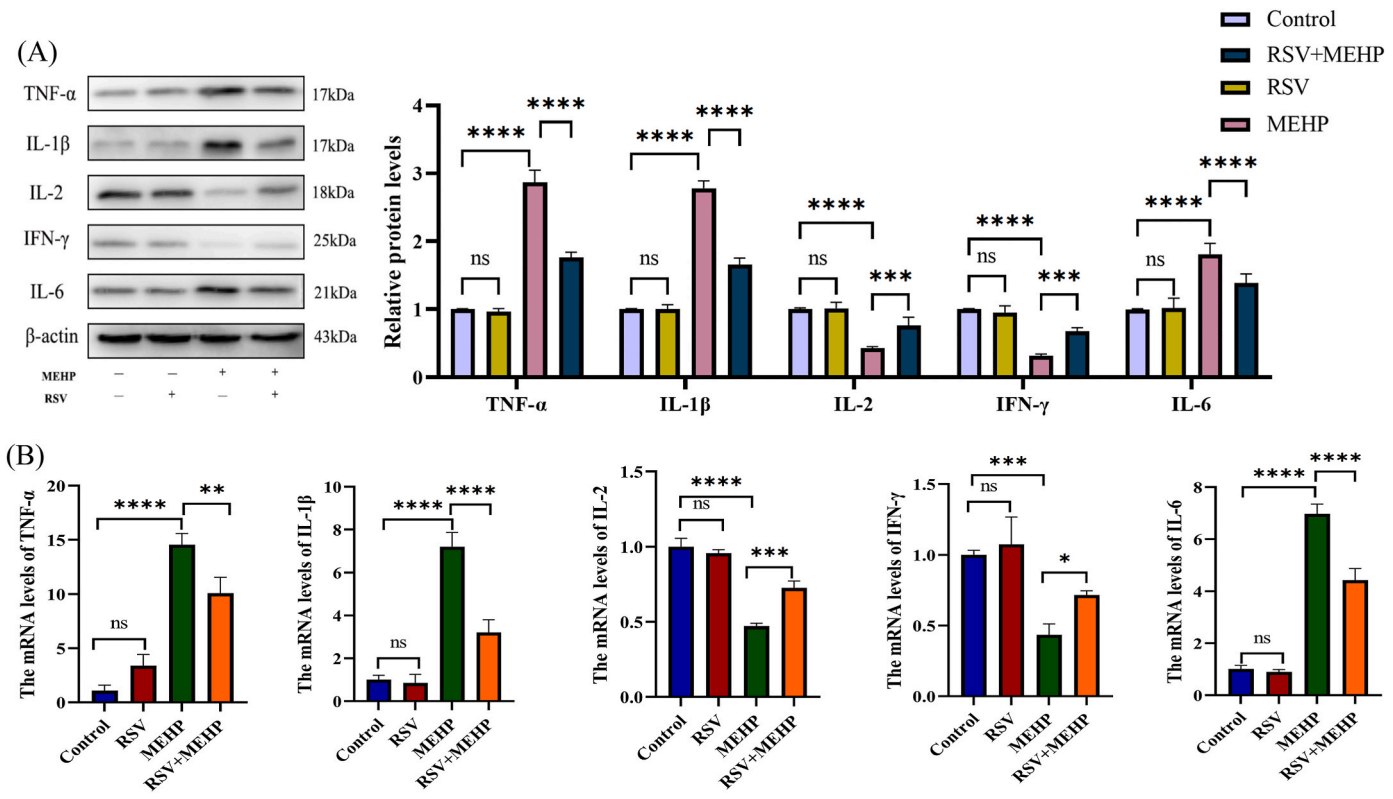

Fig. 6. RSV alleviates immune dysfunction in L8824 cells induced by MEHP exposure. (A) Expression levels of immune function-related proteins in different treatment groups. (B) Expression levels of immune function-related mRNAs in different treatment groups.

target organs of MEHP (Yuan et al., 2022). In the mammalian immune system, MEHP has been shown to have immunotoxic effects. For example, MEHP alters the immune microenvironment of adolescent rats and stimulates their secretion of pro-inflammatory cytokines (Stermer et al., 2017). Numerous studies have demonstrated that RSV lowers oxidative damage and has anti-inflammatory properties (Meng et al., 2021; Miguel et al., 2021; Wood et al., 2010). The mechanism of harm that MEHP exposure causes to L8824 cells was examined in this study, along with RSV's possible medicinal benefits. The outcomes demonstrated that MEHP could significantly increase the oxidative stress level of L8824 cells, leading to mitophagy, ferroptosis, and immune dysfunction. RSV alleviates MEHP-induced mitophagy, ferroptosis, and immunological dysfunction in L8824 cells and lowers cellular oxidative stress by regulating the Nrf2 pathway.

When the body is exposed to toxic substances, oxidative stress usually occurs (Lei et al., 2023; Gao et al., 2022c). Oxidative stress causes tissue and cellular damage by generating excess ROS that the body cannot scavenge, placing the body in a state of redox balance imbalance (Wang et al., 2023e; Deng et al., 2023; Sun et al., 2024b). It has been found that exposure to BPA and/or selenium deficiency can result in oxidative stress-induced liver inflammation in chickens (Shi et al., 2023). Oxidative stress induced in carp hepatopancreatic tissues by polystyrene microplastics abundantly present in the aquatic environment (Cui et al., 2023). Moreover, tetrabrombisphenol A exposure can produce oxidative stress, drastically raise the levels of the oxidative stress indicators MDA and ROS, inhibit the antioxidant enzymes' function, and finally result in programmed necrosis, apoptosis, and inflammation of the skeletal muscle (Zhang et al., 2023b). Numerous findings have shown that RSV has strong antioxidant properties. For example, Bi et al. found that RSV could ameliorate mecamylamine avermectin benzoate-induced hepatocyte pyroptosis and inflammation in grass carp by alleviating oxidative stress (Bi et al., 2023). RSV reduces inflammation and oxidative stress in rats with type 2 diabetes, as shown by Katarzyna Szkudelska et al. (2020). In addition, as discovered by Nurgul Atmaca et al., RSV had a protective effect on oxidative stress, hepatotoxicity, and neurotoxicity induced by sodium fluoride in rats. Our study's results, which are in line with the earlier research, showed that MEHP exposure reduced the activities of CAT, SOD, and GSH-Px in L8824 cells as well as lowered T-AOC and increased MDA concentration. After RSV treatment, the occurrence of MEHP-induced oxidative stress was significantly alleviated. Since excess ROS can induce oxidative stress, Nrf2 is an essential regulator of cell oxidative homeostasis. When oxidative stress occurs, Nrf2 is activated to protect cells from free radical damage (Wu et al., 2023). Research reveals that cadmium-induced oxidative stress alters Nrf2-Keap1 signaling and induces apoptosis in macrophages located in the head kidney of fish (Choudhury et al., 2021). Overexpression of Nrf2 can mitigate the oxidative stress and death of SH-SY5Y cells caused by Pb (Ye et al., 2015). Another investigation revealed that RSV activated the Keap-1/Nrf2 antioxidant defense system to prevent oxidative stress in obese asthmatic rats (Li et al., 2018). In line with the previous research, Keap1 dissociated from Nrf2, and Nrf2 expression increased in the nucleus of L8824 cells after exposure to MEHP in our research. After RSV treatment, the Nrf2 pathway was further activated, and a substantial quantity of Nrf2 entered the nucleus. The expression of downstream antioxidant enzymes HO-1 and NQO1 was enhanced. Mitophagy and the Nrf2 pathway are intimately associated. Repeated exposure to radon gas has been shown to alter the Nrf2 pathway in mice, which in turn causes lung damage brought on by mitophagy (Xin et al., 2022). Melatonin inhibits liver mitophagy and inflammation induced by PM2.5 by regulating the Nrf2 pathway (Zhu et al., 2023c). In this study, the expressions of mitophagy-related indicators PINK1, Parkin, Beclin1, LC3B, and ATG5 were up-regulated, and the expression of P62 was down-regulated after MEHP exposure, suggesting the occurrence of mitophagy. RSV alleviates MEHP-induced mitophagy in L8824 cells by regulating the Nrf2 pathway. The Nrf2 pathway also plays a major role in regulating ferroptosis (Dodson et al., 2019). By suppressing ferroptosis via the Nrf2 pathway, irisin averts sepsis-associated encephalopathy (Wang et al., 2022). In addition, RSV

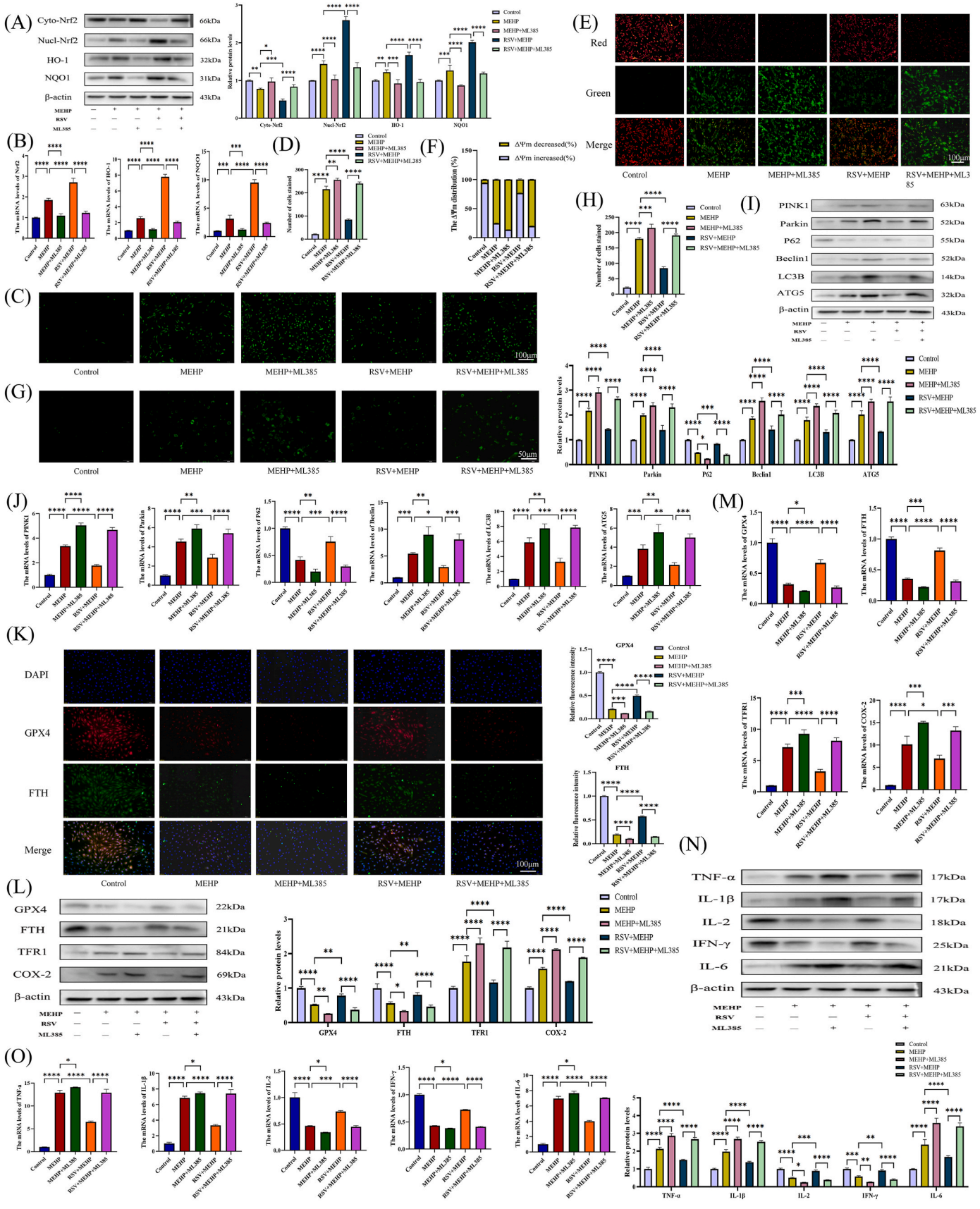

(caption on next page)

Fig. 7. RSV alleviates mitophagy, ferroptosis, and immune dysfunction of L8824 cells induced by MEHP by regulating the Nrf2 pathway. (A) The effect of inhibition of the Nrf2 pathway on the expression of Nrf2 pathway-related proteins. (B) The effect of inhibition of the Nrf2 pathway on mRNA expression related to the Nrf2 pathway. (C) The effect of inhibiting the Nrf2 pathway on ROS level. The scales in Fig. 7C are all 100 μm. (D) Quantification of Fig. 7C. (E) Effect of inhibition of the Nrf2 pathway on mitochondrial membrane potential. The scales in Fig. 7E are all 100 μm. (F) Quantification of Fig. 7E. (G) Effect of inhibition of Nrf2 pathway on autophagosome formation. The scales in Fig. 7G are all 50 μm. (H) Quantification of Fig. 7G. (I) The effect of inhibition of the Nrf2 pathway on the expression of mitophagy-related proteins. (J) Effect of inhibition of Nrf2 pathway on mRNA expression related to mitophagy. (K) Immunofluorescence double staining of GPX4 and FTH was used to detect the effect of inhibition of the Nrf2 pathway on ferroptosis. The scales in Fig. 7K are all 100 μm. (L) Effect of inhibition of Nrf2 pathway on expression of ferroptosis-related protein. (M) Effect of inhibition of Nrf2 pathway on expression of ferroptosis-related mRNA. (N) Effect of inhibition of Nrf2 pathway on expression of immune-function related proteins. (O) Effect of inhibition of Nrf2 pathway on expression of immune-function related mRNA.

prevented vomitoxin-induced ferroptosis in HepG2 cells by reducing oxidative stress and modulating Nrf2 signaling (Wang et al., 2023f). Consistent with the above studies, the expression of ferroptosis-related indicators TFR1 and COX-2 were up-regulated, and the expression of GPX4 and FTH was down-regulated after exposure to MEHP. The above was significantly improved by RSV intervention. This suggests RSV can reduce the ferroptosis of L8824 cells induced by MEHP exposure. In terms of immune regulation, Nrf2 can promote the activation of innate immunity of macrophages (Rao et al., 2022). It has been found that 4-octyl itaconate activates the Nrf2 signal to control immunological homeostasis (Zhang et al., 2022d). When immune function is abnormal, the levels of inflammatory factors are usually altered. One study found that combined exposure to emvermectin benzoate and microplastics led to increased expression of TNF-α and IL-1β proteins and decreased expression of IL-2 and IFN-γ proteins in the midgut of carp (Shi et al., 2024). It is suggested that the combined exposure of mevermectin benzoate and microplastics can cause immune dysfunction in carp midgut. Another study found that paraquat caused immune dysfunction in fish kidney cells by reducing IL-2 mRNA expression and increasing IL-6 mRNA expression (Shi et al., 2022). In our study, following exposure to MEHP, the cytokines TNF-α, IL-1β, and IL-6 showed increased expression, while IL-2 and IFN-γ showed decreased expression suggesting immune dysfunction, while RSV could alleviate MEHP-induced immune dysfunction. Finally, we further verified the effect of the Nrf2 pathway on mitophagy, ferroptosis, and immune dysfunction caused by MEHP-induced oxidative stress in L8824 cells by adding Nrf2 inhibitors. According to the experimental results, we concluded that RSV inhibited mitophagy, ferroptosis, and immune dysfunction caused by MEHP-induced oxidative stress on L8824 cell lines by activating the Nrf2 pathway. Some studies have found that excessive mitophagy can increase the iron content in the cell, which leads to the occurrence of ferroptosis (Singh et al., 2021). For example, β-amyloid protein leads to the occurrence of ferroptosis by inducing an increase in mitophagy (Li et al., 2022b). In addition, ferroptosis can induce immune dysfunction. For example, L-citrulline supplements inhibit ferroptosis-induced immune dysfunction and thymus oxidative damage (Ba et al., 2022). In the course of future research, we plan to further explore the exact association between mitophagy, ferroptosis, and immune dysfunction induced by MEHP.

In our study, MEHP induced L8824 cells to produce excessive ROS, disrupting the balance of the antioxidant system of L8824 cells and thus causing oxidative stress. L8824 cells undergoing oxidative stress exhibited a decrease in mitochondrial membrane potential, which ultimately led to the occurrence of mitophagy. Meanwhile, oxidative stress in L8824 cells also led to ferroptosis and immune dysfunction. In contrast, the addition of RSV activated the Nrf2 pathway and inhibited the occurrence of oxidative stress in L8824 cells, thereby ameliorating the MEHP-induced mitophagy, ferroptosis, and immune dysfunction. In summary, this study confirmed that RSV can alleviate the toxic effect of MEHP on L8824 cells by regulating the Nrf2 pathway. MEHP is the main metabolite of environmental pollutant DEHP. We studied the toxicity mechanism of MEHP to understand the harm of DEHP to aquatic organisms. RSV is a potential detoxification drug of MEHP, and the study of its detoxification mechanism provides a valuable scientific basis for alleviating the harm of phthalate plasticizers to aquatic organisms. The main object of this study is L8824 cells. Although the mechanism of RSV alleviating MEHP toxicity has been verified at the cellular level, there are some limitations due to the lack of validation in vivo. However, this does not mean that the value of this study is diminished; on the contrary, it lays the foundation for further research. In future studies, we will explore further by conducting in vivo experiments to validate and extend the results of this study.

CRediT authorship contribution statement

Xiaodan Wang: Writing – original draft, Software, Methodology. **Meichen Gao:** Writing – original draft, Data curation. **Xiunan Lu:** Supervision, Software, Investigation. **Yutian Lei:** Validation, Supervision. **Jiatong Sun:** Software. **Mengyao Ren:** Investigation. **Tong Xu:** Validation, Supervision. **Hongjin Lin:** Writing – review & editing, Resources, Conceptualization.

Declaration of competing interest

The authors declare that they have no known competing financial interests or personal relationships that could have appeared to influence the work reported in this paper.

Data availability

Data will be made available on request.

References

Ashari, S., Karami, M., Shokrzadeh, M., Bagheri, A., Ghandadi, M., Ranaee, M., Dashti, A., Mohammadi, H., 2022. Quercetin ameliorates Di (2-ethylhexyl) phthalate-induced nephrotoxicity by inhibiting NF-κB signaling pathway. Toxicology research 11 (2), 272–285.

Ba, T., Zhao, D., Chen, Y., Zeng, C., Zhang, C., Niu, S., Dai, H., 2022. L-citrulline supplementation restrains ferritinophagy-mediated ferroptosis to alleviate iron overload-induced thymus oxidative damage and immune dysfunction. Nutrients 14 (21).

Bi, Y., Li, X., Wei, H., Xu, S., 2023. Resveratrol improves emamectin benzoate-induced pyroptosis and inflammation of Ctenopharyngodon idellus hepatic cells by alleviating oxidative stress/endoplasmic reticulum stress. Fish Shellfish Immunol. 142, 109148.

Cai, J., Liu, P., Zhang, X., Shi, B., Jiang, Y., Qiao, S., Liu, Q., Fang, C., Zhang, Z., 2023. Micro-algal astaxanthin improves lambda-cyhalothrin-induced necroptosis and inflammatory responses via the ROS-mediated NF-κB signaling in lymphocytes of carp (Cyprinus carpio L.). Fish Shellfish Immunol. 139, 108929.

Chen, Q., Kong, Q., Tian, P., He, Y., Zhao, J., Zhang, H., Wang, G., Chen, W., 2022. Lactic acid bacteria alleviate di-(2-ethylhexyl) phthalate-induced liver and testis toxicity via their bio-binding capacity, antioxidant capacity and regulation of the gut microbiota. Environmental Pollution 305, 119197.

Choudhury, C., Mazumder, R., Kumar, R., Dhar, B., Sengupta, M., 2021. Cadmium induced oxystress alters Nrf2-Keap1 signaling and triggers apoptosis in piscine head kidney macrophages. Aquatic toxicology (Amsterdam, Netherlands) 231, 105739.

Cui, J., Zhang, Y., Liu, L., Zhang, Q., Xu, S., Guo, M.-y., 2023. Polystyrene microplastics induced inflammation with activating the TLR2 signal by excessive accumulation of ROS in hepatopancreas of carp (Cyprinus carpio). Ecotoxicol. Environ. Saf. 251, 114539.

Deng, X., Yu, T., Gao, M., Wang, J., Sun, W., Xu, S., 2023. Sodium selenite (Na2SeO3) attenuates T-2 toxin-induced iron death in LMH cells through the ROS/PI3K/AKT/Nrf2 pathway. Food Chem. Toxicol. 182, 114185.

Dodson, M., Castro-Portuguez, R., Zhang, D.D., 2019. NRF2 plays a critical role in mitigating lipid peroxidation and ferroptosis. Redox Biol. 23, 101107.

Dong, Q., Wang, J., Liu, J., Zhang, L., Xu, Z., Kang, Y., Xue, P., 2023. Manganese-based redox homeostasis disruptor for inducing intense ferroptosis/apoptosis through xCT inhibition and oxidative stress injury. Adv. Healthcare Mater. 12 (28), e2301453.

Dueñas-Moreno, J., Vázquez-Tapia, I., Mora, A., Cervantes-Avilés, P., Mahlknecht, J., Capparelli, M.V., Kumar, M., Wang, C., 2023. Occurrence, ecological and health risk

assessment of phthalates in a polluted urban river used for agricultural land irrigation in central Mexico. Environ. Res., 117454
Erkekoğlu, P., Rachidi, W., De Rosa, V., Giray, B., Favier, A., Hincal, F., 2010. Protective effect of selenium supplementation on the genotoxicity of di(2-ethylhexyl)phthalate and mono(2-ethylhexyl)phthalate treatment in LNCaP cells. Free radical biology & medicine 49 (4), 559–566.
Fu, L., Song, S., Luo, X., Luo, Y., Guo, C., Liu, Y., Luo, X., Zeng, L., Tan, L., 2023. Unraveling the contribution of dietary intake to human phthalate internal exposure. Environmental pollution (Barking, Essex : 1987) 337, 122580.
Gao, M., Zhu, H., Guo, J., Lei, Y., Sun, W., Lin, H., 2022a. Tannic acid through ROS/TNF-α/TNFR 1 antagonizes atrazine induced apoptosis, programmed necrosis and immune dysfunction of grass carp hepatocytes. Fish Shellfish Immunol. 131, 312–322.
Gao, M., Yang, N., Lei, Y., Zhang, W., Liu, H., Lin, H., 2022b. Tannic acid antagonizes atrazine exposure-induced autophagy and DNA damage crosstalk in grass carp hepatocytes via NO/iNOS/NF-κB signaling pathway to maintain stable immune function. Fish Shellfish Immunol. 131, 1075–1084.
Gao, M., Zhu, H., Guo, J., Lei, Y., Sun, W., Lin, H., 2022c. Tannic acid through ROS/TNF-α/TNFR 1 antagonizes atrazine induced apoptosis, programmed necrosis and immune dysfunction of grass carp hepatocytes. Fish Shellfish Immunol. 131, 312–322.
Griñán-Ferré, C., Bellver-Sanchis, A., Izquierdo, V., Corpas, R., Roig-Soriano, J., Chillón, M., Andres-Lacueva, C., Somogyvári, M., Sőti, C., Sanfeliu, C., Pallàs, M., 2021. The pleiotropic neuroprotective effects of resveratrol in cognitive decline and Alzheimer's disease pathology: from antioxidant to epigenetic therapy. Ageing Res. Rev. 67, 101271.
Hong, Y., Zhou, X., Li, Q., Chen, J., Wei, Y., Shen, L., Long, C., Wu, S., Wei, G., 2023a. Epigallocatechin gallate alleviates mono-2-ethylhexyl phthalate-induced male germ cell pyroptosis by inhibiting the ROS/mTOR/NLRP3 pathway. Toxicol. Vitro 91, 105626.
Hong, Y., Zhou, X., Li, Q., Chen, J., Wei, Y., Wang, S., Zheng, X., Zhao, J., Yu, C., Pei, J., Zhang, J., Long, C., Shen, L., Wu, S., Wei, G., 2023b. Wnt10a downregulation contributes to MEHP-induced disruption of self-renewal and differentiation balance and proliferation inhibition in GC-1 cells: insights from multiple transcriptomic profiling. Environmental Pollution 333, 122091.
Hou, L., Wang, D., Yin, K., Zhang, Y., Lu, H., Guo, T., Li, J., Zhao, H., Xing, M., 2022. Polystyrene microplastics induce apoptosis in chicken testis via crosstalk between NF-κB and Nrf2 pathways. Comparative biochemistry and physiology. Toxicology & pharmacology : CBP 262, 109444.
Huang, J., Zhu, Y., Li, S., Jiang, H., Chen, N., Xiao, H., Liu, J., Liang, D., Zheng, Q., Tang, J., Meng, X., 2023. Licochalcone B confers protective effects against LPS-Induced acute lung injury in cells and mice through the Keap1/Nrf2 pathway. Redox Rep. 28 (1), 2243423.
Kasai, S., Kokubu, D., Mizukami, H., Itoh, K., 2023. Mitochondrial reactive oxygen species, insulin resistance, and nrf2-mediated oxidative stress response-toward an actionable strategy for anti-aging. Biomolecules 13 (10).
Kim, D., Oh, E., Kim, H., Baek, S.M., Cho, J., Kim, E.-H., Choi, S., Bian, Y., Kim, W., Bae, O.-N., 2023. Mono-(2-ethylhexyl)-phthalate potentiates methylglyoxal-induced blood–brain barrier damage via mitochondria-derived oxidative stress and bioenergetic perturbation. Food Chem. Toxicol. 179, 113985.
Kotowska, U., Kapelewska, J., Sawczuk, R., 2020. Occurrence, removal, and environmental risk of phthalates in wastewaters, landfill leachates, and groundwater in Poland. Environmental Pollution 267, 115643.
Lai, X., Pei, Q., Song, X., Zhou, X., Yin, Z., Jia, R., Zou, Y., Li, L., Yue, G., Liang, X., Yin, L., Lv, C., Jing, B., 2016. The enhancement of immune function and activation of NF-κB by resveratrol-treatment in immunosuppressive mice. Int. Immunopharm. 33, 42–47.
Lei, Y., Xu, T., Sun, W., Wang, X., Gao, M., Lin, H., 2023. Evodiamine alleviates DEHP-induced hepatocyte pyroptosis, necroptosis and immunosuppression in grass carp through ROS-regulated TLR4/MyD88/NF-κB pathway. Fish Shellfish Immunol. 140, 108995.
Lei, Y., Sun, W., Xu, T., Shan, J., Gao, M., Lin, H., 2024. Selenomethionine modulates the JAK2/STAT3/A20 pathway through oxidative stress to alleviate LPS-induced pyroptosis and inflammation in chicken hearts. Biochimica et biophysica acta. General subjects 1868 (4), 130564.
Li, X.N., Ma, L.Y., Ji, H., Qin, Y.H., Jin, S.S., Xu, L.X., 2018. Resveratrol protects against oxidative stress by activating the Keap-1/Nrf2 antioxidant defense system in obese-asthmatic rats. Exp. Ther. Med. 16 (6), 4339–4348.
Li, T., Tan, Y., Ouyang, S., He, J., Liu, L., 2022a. Resveratrol protects against myocardial ischemia-reperfusion injury via attenuating ferroptosis. Gene 808, 145968.
Li, J., Li, M., Ge, Y., Chen, J., Ma, J., Wang, C., Sun, M., Wang, L., Yao, S., Yao, C., 2022b. β-amyloid protein induces mitophagy-dependent ferroptosis through the CD36/PINK/PARKIN pathway leading to blood-brain barrier destruction in Alzheimer's disease. Cell Biosci. 12 (1), 69.
Li, L., Li, W., Liu, Y., Jin, X., Yu, Y., Lin, H., 2023a. TBBPA and lead co-exposure induces grass carp liver cells apoptosis via ROS/JAK2/STAT3 signaling axis. Fish Shellfish Immunol. 142, 109100.
Li, J., Yin, K., Hou, L., Zhang, Y., Lu, H., Ma, C., Xing, M., 2023b. Polystyrene microplastics mediate inflammatory responses in the chicken thymus by Nrf2/NF-κB pathway and trigger autophagy and apoptosis. Environ. Toxicol. Pharmacol. 100, 104136.
Li, X.N., Shang, N.Y., Kang, Y.Y., Sheng, N., Lan, J.Q., Tang, J.S., Wu, L., Zhang, J.L., Peng, Y., 2024. Caffeic acid alleviates cerebral ischemic injury in rats by resisting ferroptosis via Nrf2 signaling pathway. Acta pharmacologica Sinica. 45 (2), 248–267.
Li, X., Zhu, Y., Zhao, T., Zhang, X., Qian, H., Wang, J., Miao, X., Zhou, L., Li, N., Ye, L., 2023d. Role of COX-2/PGE2 signaling pathway in the apoptosis of rat ovarian granulosa cells induced by MEHP. Ecotoxicol. Environ. Saf. 254, 114717.
Li, J.Y., Guo, J.L., Yi, J.F., Liu, L.Y., Zeng, L.X., Guo, Y., 2024. Widespread phthalate esters and monoesters in the aquatic environment: distribution, bioconcentration, and ecological risks. J. Hazard Mater. 477, 135201.
Lim, J.O., Song, K.H., Lee, I.S., Lee, S.J., Kim, W.I., Pak, S.W., Shin, I.S., Kim, T., 2021. Cimicifugae rhizoma extract attenuates oxidative stress and airway inflammation via the upregulation of Nrf2/HO-1/NQO1 and downregulation of NF-κB phosphorylation in ovalbumin-induced asthma. Antioxidants 10 (10).
Liu, Y., Huo, W.-B., Deng, J.-Y., Tang, Q.-P., Wang, J.-X., Liao, Y.-L., Gou, D., Pei, D.-S., 2023a. Neurotoxicity and the potential molecular mechanisms of mono-2-ethylhexyl phthalic acid (MEHP) in zebrafish. Ecotoxicol. Environ. Saf. 265, 115516.
Liu, H., Wang, K., Han, D., Sun, W., Xu, S., 2023b. Co-exposure of avermectin and imidacloprid induces DNA damage, pyroptosis, and immune dysfunction in epithelioma papulosum cyprini cells via ROS-mediated Keap1/Nrf2/TXNIP axis. Fish Shellfish Immunol. 140, 108985.
Lv, X., Ren, M., Xu, T., Gao, M., Liu, H., Lin, H., 2023. Selenium alleviates lead-induced CIK cells pyroptosis and inflammation through IRAK1/TAK1/IKK pathway. Fish Shellfish Immunol. 142, 109101.
Meng, T., Xiao, D., Muhammed, A., Deng, J., Chen, L., He, J., 2021. Anti-inflammatory action and mechanisms of resveratrol. Molecules 26 (1).
Miao, Z., Miao, Z., Feng, S., Xu, S., 2023. Chlorpyrifos-mediated mitochondrial calcium overload induces EPC cell apoptosis via ROS/AMPK/ULK1. Fish Shellfish Immunol. 141, 109053.
Miguel, C.A., Noya-Riobó, M.V., Mazzone, G.L., Villar, M.J., Coronel, M.F., 2021. Antioxidant, anti-inflammatory and neuroprotective actions of resveratrol after experimental nervous system insults. Special focus on the molecular mechanisms involved. Neurochem. Int. 150, 105188.
Qiu, W., Ye, J., Su, Y., Zhang, X., Pang, X., Liao, J., Wang, R., Zhao, C., Zhang, H., Hu, L., Tang, Z., Su, R., 2023. Co-exposure to environmentally relevant concentrations of cadmium and polystyrene nanoplastics induced oxidative stress, ferroptosis and excessive mitophagy in mice kidney. Environmental Pollution 333, 121947.
Rao, J., Qiu, J., Ni, M., Wang, H., Wang, P., Zhang, L., Wang, Z., Liu, M., Cheng, F., Wang, X., Lu, L., 2022. Macrophage nuclear factor erythroid 2-related factor 2 deficiency promotes innate immune activation by tissue inhibitor of metalloproteinase 3-mediated RhoA/ROCK pathway in the ischemic liver. Hepatology 75 (6), 1429–1445.
Shahcheraghi, S.H., Salemi, F., Small, S., Syed, S., Salari, F., Alam, W., Cheang, W.S., Saso, L., Khan, H., 2023. Resveratrol regulates inflammation and improves oxidative stress via Nrf2 signaling pathway: therapeutic and biotechnological prospects. Phytother Res. : PTR 37 (4), 1590–1605.
Shan, W., Niu, W., Lin, Q., Shen, Y., Shen, F., Lou, K., Zhang, Y., 2023. Bisphenol S exposure promotes cell apoptosis and mitophagy in murine osteocytes by regulating mtROS signaling. Microsc. Res. Tech. 86 (4), 481–493.
Shi, X., Zhu, W., Chen, T., Cui, W., Li, X., Xu, S., 2022. Paraquat induces apoptosis, programmed necrosis, and immune dysfunction in CIK cells via the PTEN/PI3K/AKT axis. Fish Shellfish Immunol. 130, 309–316.
Shi, X., Xu, T., Li, X., Sun, X., Zhang, W., Liu, X., Wang, Y., Zhang, Y., Xu, S., 2023. ROS mediated pyroptosis-M1 polarization crosstalk participates in inflammation of chicken liver induced by bisphenol A and selenium deficiency. Environmental Pollution 324, 121392.
Shi, X., Xu, T., Gao, M., Bi, Y., Wang, J., Yin, Y., Xu, S., 2024. Combined exposure of emamectin benzoate and microplastics induces tight junction disorder, immune disorder and inflammation in carp midgut via lysosome/ROS/ferroptosis pathway. Water Res. 257, 121660.
Singh, L.P., Yumnamcha, T., Devi, T.S., 2021. Mitophagy, ferritinophagy and ferroptosis in retinal pigment epithelial cells under high glucose conditions: implications for diabetic retinopathy and age-related retinal diseases. JOJ ophthalmology 8 (5), 77–85.
Song, J., Wang, H., Sheng, J., Zhang, W., Lei, J., Gan, W., Cai, F., Yang, Y., 2023. Vitexin attenuates chronic kidney disease by inhibiting renal tubular epithelial cell ferroptosis via NRF2 activation. Molecular Medicine 29 (1), 147.
Stermer, A.R., Murphy, C.J., Ghaffari, R., Di Bona, K.R., Voss, J.J., Richburg, J.H., 2017. Mono-(2-ethylhexyl) phthalate-induced Sertoli cell injury stimulates the production of pro-inflammatory cytokines in Fischer 344 rats. Reprod. Toxicol. 69, 150–158.
Sun, W., Lei, Y., Jiang, Z., Wang, K., Liu, H., Xu, T., 2024a. BPA and low-Se exacerbate apoptosis and mitophagy in chicken pancreatic cells by regulating the PTEN/PI3K/AKT/mTOR pathway. J. Adv. Res.
Sun, W., Xu, T., Lin, H., Yin, Y., Xu, S., 2024b. BPA and low-Se exacerbate apoptosis and autophagy in the chicken bursa of Fabricius by regulating the ROS/AKT/FOXO1 pathway. The Science of the total environment 908, 168424.
Szkudelska, K., Okulicz, M., Hertig, I., Szkudelski, T., 2020. Resveratrol ameliorates inflammatory and oxidative stress in type 2 diabetic Goto-Kakizaki rats. Biomedicine & pharmacotherapy = Biomedecine & pharmacotherapie 125, 110026.
Wang, J., Zhu, Q., Wang, Y., Peng, J., Shao, L., Li, X., 2022. Irisin protects against sepsis-associated encephalopathy by suppressing ferroptosis via activation of the Nrf2/GPX4 signal axis. Free radical biology & medicine 187, 171–184.
Wang, K., Liu, H., Sun, W., Guo, J., Jiang, Z., Xu, S., Miao, Z., 2023a. Eucalyptol alleviates avermectin exposure-induced apoptosis and necroptosis of grass carp hepatocytes by regulating ROS/NLRP3 axis. Aquat. Toxicol. 264, 106739.
Wang, X., Tian, X., Yan, H., Zhu, T., Ren, H., Zhou, Y., Zhao, D., Xu, D., Lian, X., Fang, L., Yu, Y., Liao, X., Liu, Y., Sun, J., 2023b. Exposure to salinomycin dysregulates interplay between mitophagy and oxidative response to damage the porcine jejunal cells. Sci. Total Environ. 900, 166441.

Wang, L., Xu, R., Huang, C., Yi, G., Li, Z., Zhang, H., Ye, R., Qi, S., Huang, G., Qu, S., 2023c. Targeting the ferroptosis crosstalk: novel alternative strategies for the treatment of major depressive disorder. General psychiatry 36 (5), e101072.
Wang, P., Yang, Y., Guo, J., Ma, T., Hu, Y., Huang, L., He, Y., Xi, J., 2024. Resveratrol Inhibits Zinc Deficiency-Induced Mitophagy and Exerts Cardiac Cytoprotective Effects. Biological trace element research 202 (4), 1669–1682.
Wang, J., Yin, Y., Zhang, Q., Deng, X., Miao, Z., Xu, S., 2023e. HgCl(2) exposure mediates pyroptosis of HD11 cells and promotes M1 polarization and the release of inflammatory factors through ROS/Nrf2/NLRP3. Ecotoxicol. Environ. Saf. 269, 115779.
Wang, P., Yao, Q., Zhu, D., Yang, X., Chen, Q., Lu, Q., Liu, A., 2023f. Resveratrol protects against deoxynivalenol-induced ferroptosis in HepG2 cells. Toxicology 494, 153589.
Wang, X., Sun, J., Xu, T., Lei, Y., Gao, M., Lin, H., 2024. Resveratrol alleviates imidacloprid-induced mitochondrial apoptosis, necroptosis, and immune dysfunction in chicken lymphocyte lines by inhibiting the ROS/MAPK signaling pathway. Environ. Toxicol. 39 (4), 2052–2063.
Wood, L.G., Wark, P.A., Garg, M.L., 2010. Antioxidant and anti-inflammatory effects of resveratrol in airway disease. Antioxidants Redox Signal. 13 (10), 1535–1548.
Wu, H., Li, H., Huo, H., Li, X., Zhu, H., Zhao, L., Liao, J., Tang, Z., Guo, J., 2023. Effects of terbuthylazine on myocardial oxidative stress and ferroptosis via Nrf2/HO-1 signaling pathway in broilers. Pestic. Biochem. Physiol. 197, 105698.
Xin, L., Sun, J., Zhai, X., Chen, X., Wan, J., Tian, H., 2022. Repeated radon exposure induced lung damage via oxidative stress-mediated mitophagy in human bronchial epithelial cells and mice. Environ. Toxicol. Pharmacol. 90, 103812.
Xing, D., Ma, Y., Lu, M., Liu, W., Zhou, H., 2023. Paeoniflorin alleviates hypoxia/reoxygenation injury in HK-2 cells by inhibiting apoptosis and repressing oxidative damage via Keap1/Nrf2/HO-1 pathway. BMC Nephrol. 24 (1), 314.
Xu, Q., Zhou, L., Ri, H., Li, X., Zhang, X., Qi, W., Ye, L., 2022a. Role of estrogen receptors in thyroid toxicity induced by mono (2-ethylhexyl) phthalate via endoplasmic reticulum stress: an in vitro mechanistic investigation. Environ. Toxicol. Pharmacol. 96, 104007.
Xu, T., Liu, Q., Chen, D., Liu, Y., 2022b. Atrazine exposure induces necroptosis through the P450/ROS pathway and causes inflammation in the gill of common carp (Cyprinus carpio L.). Fish Shellfish Immunol. 131, 809–816.
Yang, S., Chen, M., Meng, J., Hao, C., Xu, L., Wang, J., Chen, J., 2024. Melatonin alleviates di-butyl phthalate (DBP)-induced ferroptosis of mouse leydig cells via inhibiting Sp2/VDAC2 signals. Environ. Res. 247, 118221.
Ye, F., Li, X., Li, L., Lyu, L., Yuan, J., Chen, J., 2015. The role of Nrf2 in protection against Pb-induced oxidative stress and apoptosis in SH-SY5Y cells. Food Chem. Toxicol. : an international journal published for the British Industrial Biological Research Association 86, 191–201.
Yin, Y., Xu, N., Shi, Y., Zhou, B., Sun, D., Ma, B., Xu, Z., Yang, J., Li, C., 2021. Astaxanthin protects dendritic cells from lipopolysaccharide-induced immune dysfunction. Mar. Drugs 19 (6).
Yuan, Y.-Z., Ye, C., Sun, J.-H., Hu, M.-Y., Huo, S.-J., Zhu, Y.-T., Xiang, S.-Y., Yu, S.-Q., 2022. Toxicokinetics of mono-(2-ethylhexyl) phthalate with low-dose exposure applying fluorescence tracing technique. Toxicol. Appl. Pharmacol. 434, 115814.
Zhang, Y.-J., Guo, J.-L., Xue, J.-c., Bai, C.-L., Guo, Y., 2021. Phthalate metabolites: characterization, toxicities, global distribution, and exposure assessment. Environmental Pollution 291, 118106.
Zhang, X., Qi, W., Xu, Q., Li, X., Zhou, L., Ye, L., 2022a. Di(2-ethylhexyl) phthalate (DEHP) and thyroid: biological mechanisms of interference and possible clinical implications. Environ. Sci. Pollut. Control Ser. 29 (2), 1634–1644.
Zhang, Y., Hui, J., Xu, Y., Ma, Y., Sun, Z., Zhang, M., Nie, L., Ye, L., 2022b. MEHP promotes liver fibrosis by down-regulating STAT5A in BRL-3A hepatocytes. Chemosphere 295, 133925.
Zhang, F., Zhen, H., Cheng, H., Hu, F., Jia, Y., Huang, B., Jiang, M., 2022c. Di-(2-ethylhexyl) phthalate exposure induces liver injury by promoting ferroptosis via downregulation of GPX4 in pregnant mice. Front. Cell Dev. Biol. 10, 1014243.
Zhang, P., Wang, Y., Yang, W., Yin, Y., Li, C., Ma, X., Shi, L., Li, R., Tao, K., 2022d. 4-Octyl itaconate regulates immune balance by activating Nrf2 and negatively regulating PD-L1 in a mouse model of sepsis. Int. J. Biol. Sci. 18 (16), 6189–6209.
Zhang, Y., Qian, H., Wang, J., Zhu, Y., Miao, X., Li, X., Yin, J., Zhang, R., Ye, J., Huo, C., Zhao, W., Ye, L., 2023a. Di-(2-ethylhexyl) phthalate (DEHP) promoted hepatic lipid accumulation by activating Notch signaling pathway. Environ. Toxicol. 38 (7), 1628–1640.
Zhang, Q., Wang, S., Wang, F., Guo, M., Xu, S., 2023b. TBBPA induces inflammation, apoptosis, and necrosis of skeletal muscle in mice through the ROS/Nrf2/TNF-α signaling pathway. Environmental Pollution 317, 120745.
Zhao, E., Xiong, X., Li, X., Hu, H., Wu, C., 2024. Effect of biofilm forming on the migration of di(2-ethylhexyl)phthalate from PVC plastics. Environmental science & technology 58 (14), 6326–6334.
Zheng, S., Jin, X., Chen, M., Shi, Q., Zhang, H., Xu, S., 2019. Hydrogen sulfide exposure induces jejunum injury via CYP450s/ROS pathway in broilers. Chemosphere 214, 25–34.
Zhu, J., Sun, R., Sun, K., Yan, C., Jiang, J., Kong, F., Shi, J., 2023a. The deubiquitinase USP11 ameliorates intervertebral disc degeneration by regulating oxidative stress-induced ferroptosis via deubiquitinating and stabilizing Sirt3. Redox Biol. 62, 102707.
Zhu, L., Li, Y., Qiu, L., Chen, X., Guo, B., Li, H., Qi, P., 2023b. Screening of genes encoding proteins that interact with Nrf2: probing a cDNA library from Mytilus coruscus using a yeast two-hybrid system. Fish Shellfish Immunol. 142, 109112.
Zhu, L., Zhang, Q., Hua, C., Ci, X., 2023c. Melatonin alleviates particulate matter-induced liver fibrosis by inhibiting ROS-mediated mitophagy and inflammation via Nrf2 activation. Ecotoxicol. Environ. Saf. 268, 115717.